INFORMATION TO USERS

This manuscript has been reproduced from the microfilm master. UMI films the text directly from the original or copy submitted. Thus, some thesis and dissertation copies are in typewriter face, while others may be from any type of computer printer.

The quality of this reproduction is dependent upon the quality of the copy submitted. Broken or indistinct print, colored or poor quality illustrations and photographs, print bleedthrough, substandard margins, and improper alignment can adversely affect reproduction.

In the unlikely event that the author did not send UMI a complete manuscript and there are missing pages, these will be noted. Also, if unauthorized copyright material had to be removed, a note will indicate the deletion.

Oversize materials (e.g., maps, drawings, charts) are reproduced by sectioning the original, beginning at the upper left-hand corner and continuing from left to right in equal sections with small overlaps. Each original is also photographed in one exposure and is included in reduced form at the back of the book.

Photographs included in the original manuscript have been reproduced xerographically in this copy. Higher quality 6" x 9" black and white photographic prints are available for any photographs or illustrations appearing in this copy for an additional charge. Contact UMI directly to order.

UMI

A Bell & Howell Information Company
300 North Zeeb Road, Ann Arbor MI 48106-1346 USA
313/761-4700 800/521-0600

MICROPROCESSOR CONTROL OF HIGH-SPEED IMAGING SYSTEM

The members of the Committee approve the masters thesis of Xijing Liu

Frank K. Lu
Co-Supervising professor

Roger S. Walker
Co-Supervising professor

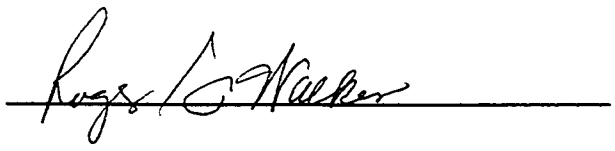

David Chenho Kung

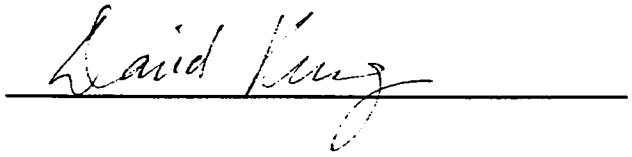

MICROPROCESSOR CONTROL OF HIGH-SPEED IMAGING SYSTEM

by

XIJING LIU

Presented to the Faculty of the Graduate School of

The University of Texas at Arlington in Partial Fulfillment

of the Requirements

for the Degree of

MASTER OF SCIENCE IN COMPUTER SCIENCE AND ENGINEERING

THE UNIVERSITY OF TEXAS AT ARLINGTON

May 1996

ACKOWLEDGMENTS

I would like to express my sincere appreciation to my supervising professor, Dr. Frank K. Lu, for his guidance, assistance, and patience during the two-year research.

Special appreciation is extended to Dr. Roger S. Walker for serving as my co-major professor and guidance of the microprocessor design. Special thanks are also extended to Dr. David Chenho Kung for serving on my graduate committee.

I would like to thank Mr. Jim H. Holland, Xiuyan Zhang, Binu Kurian, Vikas Rangarajan, and Boon Hun Tan for their help during the program.

This project is supported by the Texas Higher Education Coordinating Board's Advanced Research Program under project No. 003656-004.

April 8, 1996

ABSTRACT

MICROPROCESSOR CONTROL OF HIGH-SPEED IMAGING SYSTEM

Publication No. _____

Xijing Liu, M. S.

The University of Texas at Arlington, 1996

Supervising Professors: Frank K. Lu and Roger S. Walker

A Cranz-Schardin high-speed camera with a speed of one million frames per second has been successfully developed. LEDs as light sources, the innovative design of an efficient light-gathering system, and microprocessor control of synchronization are among other features of this camera. Using geometric optics, the design principle for the Cranz-Schardin camera is systematically addressed in the literature for the first time. An MC68000 microprocessor with a high speed A/D converter is applied for the synchronization control. With the WR-RD mode of ADC0820 A/D converter, 1.5 μs conversion time is achieved. Port A and port B of PI/T are configured in Mode 0, submode 1X to read input data instantaneously and output control signal in single-buffered mode. TCR is programmed in interrupt after time-out mode to exercise a wide range of time delay. The performance of the camera is examined through a cavitation experiment.

TABLE OF CONTENTS

LIST OF FIGURES

LIST OF TABLES

CHAPTER ONE

INTRODUCTION

A conventional high-speed camera such as a framing camera employs a high speed rotating mechanical-optical component to sweep images on a stationary strip of film that is fastened to a cylindrical surface [1, 2]. With all of its advantages, this kind of high-speed camera has the following shortcomings: (1) due to the high speed rotating mechanical-optical component, its design and manufacture are complicated and the cost is very high, and (2) a lot of dark room work is needed to develop the negative film. A low-cost high-speed camera that uses instant film can address these shortcomings.

In 1929, Cranz and Schardin developed a technique for taking a short series of photographs [3]. Basically, the Cranz-Schardin technique utilizes an array of point light sources which is fired in a time-controlled sequence to provide both the light and the shutter action required to stop image movement during a dynamic event. This technique is most effective in transmitted light photography. The principle of their method is illustrated in figure 1 [4]. Framing rates up to one million frames per second can be achieved, and the framing rate can be varied according to a predetermined schedule during the dynamic event. Non-equal time interval photography is also feasible. In the Cranz-Schardin system, image-splitting is achieved through the arrangement of light sources and the

optical system. Frame rate and exposure time depend on the response time of the light sources and the drive circuit. The exposure time is independent of framing rate. The image plane is flat to which an instant film can be placed. With these features, the Cranz-Schardin system is suitable for developing a high speed, low cost, instant image high-speed camera.

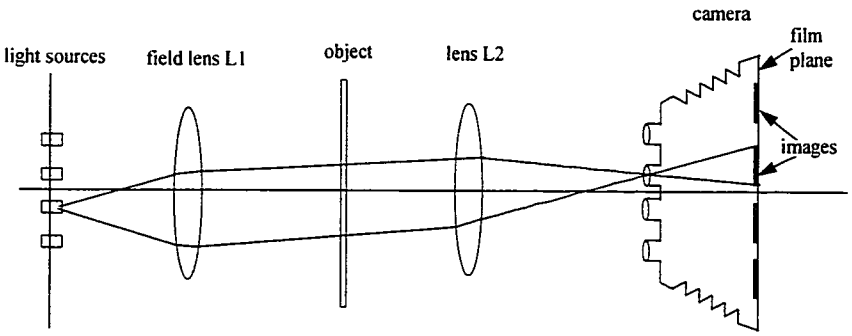

Figure 1.1 Princilpe of Cranz-Shardin camera

During the study of cavitation at The University of Texas at Arlington, to meet the demand of high speed, low cost, and instant image for recording the high speed process of the interaction between shock and bubble, a Cranz-Schardin high-speed camera with a speed of one million frames per second has been successfully developed. The light sources

play an especially important role in the Cranz-Schardin system because of its dual function as light source and shutter. Since the development of the original Cranz-Schardin system, various kinds of point light sources have been used. After review of the features of various light sources, LEDs are chosen for the system due to the fact that they are cheap, compact and small, and easy to control. By nature, LEDs are weak light sources. For this reason, a carefully designed, light-gathering power optical system has been developed. While conventional high-speed camera design theory and method are complete, unfortunately, the imaging mechanism of Cranz-Schardin optical system is poorly addressed in the literature. In the following chapters, after a review of light sources used in Cranz-Schardin system, the Cranz-Schardin optical system is analyzed in detail based on geometric optics theory. This analysis serves the purpose of providing a design guide for developing the Cranz-Schardin high-speed camera which is currently not commercially available. Synchronization is critical to high-speed photography. It is more important for the Cranz-Schardin camera because the Cranz-Schardin camera captures relatively few frames at an extremely high framing rate. An MC68000 microprocessor control system has been developed to achieve accurate, precise, and flexible synchronization. The design of the microprocessor control system is also treated in detail. Finally, we have used this high-speed photographic system to study the high speed process of the interaction between a shock and a bubble. The experiment set-up and experiment procedures are also described. Preliminary experiment results of cavitation study are presented.

CHAPTER TWO

LIGHT SOURCES OF THE CRANZ-SCHARDIN CAMERA

The most significant feature in the design of Cranz-Schardin cameras is in the light sources [5]. The camera requires an array of point light sources which functions as illumination and shutter, with a combination of lenses to separate the images. The point light sources should have good response, be easy to control, and their dimensions should be small. Since the development of Cranz-Schardin camera, various kinds of light sources have been used. In this chapter, several point light sources are briefly reviewed. This review provides the rationale for choosing LEDs as light sources. The properties of the LEDs and pulse generator are also discussed in some detail.

2.1 Spark Gap and Its Drive Circuits

The highly intense short-duration spark produced by an electric discharge provides the basis for many types of photography. The spark gap is originally used in the Cranz-Schardin camera. Physically, the spark gaps consist of two solid brass spheres (1/2-in. dia.) spaced with a 1/2-in gap. In the ready mode of operation, both electrodes of each gap are at the same potential; hence, the stability of the system is excellent.

A series connected L-C line to energize an array of spark gaps is illustrated in

figure 2.1 [6]. The capacitors C1, C2, C3 .... and C1*, C2*, C3* .... are charged to 15 kV DC with a 5 mA DC power supply. The firing of the spark gaps G1, G2, G3, ... is initiated at a preselected time after the beginning of the dynamic event by applying a 15-kV pulse to the trigger gap. When the trigger gap is fired, the capacitor C1* discharges through the gap to below ground potential. When the voltage on C1* becomes sufficiently negative, spark gap G1 breaks down and the energy stored in capacitor C1 discharges through the spark gap G1 producing a short intense flash of light.

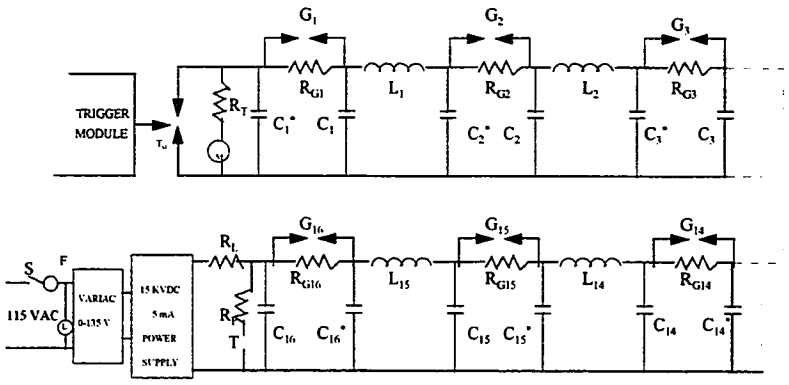

Figure 2.1. An array of spark gaps energinized by a series connected L-C line

The spark gap has several shortcomings. Spatial, temporal and intensity jitters, as well as the difficulties with control and screening due to the generated electromagnetic disturbances are particular disadvantages [7]. The life time of the system is limited due to electrode erosion. Furthermore, the high voltage and charge require special safety

precautions. The heavy weight and large dimensions create additional inconveniences. It can only operate in a pulse flash mode, and adjustments of the optical setup is very difficult.

2.2 Ruby Laser and Semiconductor Laser

Multiple ruby lasers have been used in Cranz-Schardin cameras [8]. Their advantages include: (1) very short exposure times (30 ns), (2) extremely high framing rates (10 million frames per second), and (3) the light output from the Q-switched laser much greater than that of spark gaps. However, the cost is too expensive. The cost for a 12-frame camera is about $0.4 million [9].

Pulsed semiconductor lasers have also been used [10]. Their light output power ranges to some hundred watts and their pulse widths can be as short as a few nanoseconds. However, the speckle effect caused by the high coherence of laser light may have a negative influence on the image quality. Other disadvantages, which cause some inconveniences when adjusting the optical setup, are that pulse laser diodes emit invisible light (800-904 nm) and cannot be operated in the continuous wave mode.

2.3 LEDs

Recently developed GaAlAs diode can emit intense red light of wavelength 660 nm. These cheap, compact, and small light sources are effective for the investigation and visualization of fast processes by optical methods.

During the late 1980s, Stasicki et al. [11, 12, 13], have experimented with the use

of LEDs as light sources for a Cranz-Schardin camera. Normally, an LED is operated under 20 mA current and the maximum light output power about 5 mW. The wavelength of emission is 660 nm with a spectral width of 27 nm. Stasicki et al., found that the LED can be operated at current pulses up to 10 A with pulse widths between 50 ns and 2 μs emitting about 1 W light power, a 200-fold increase over continuous operation mode. The resulting light pulse energy is up to 2 μJ. The light pulse half-width is about 35 ns when driving the LED with a 50 ns current pulse. These operating conditions, far beyond the limits specified by the manufacturers, caused no observable degradation of the LED properties. Stasick et al., recommended that pulse currents higher than 10 A should be avoided. They developed a moderate LED light pulse energy system for a Cranz-Schardin light source system. Unfortunately, LEDs are inherently weak light emitting. For some applications, more than one LED is needed, and they are coupled by optical fibers. Although there are some shortcomings, LEDs are good light sources for a Cranz-Schardin camera because of their advantages of fast response and ease of control.

2.4 LED Properties and Pulse Generator

Hewlett Packard HLMA-CH00 LEDs using newly developed aluminum indium gallium phosphide (AlInGaP) technology are used in our system. Table 1 shows some technical data. The main advantages of this LED are that it has a very high luminous intensity, typically 3000 mcd at a current of 20 mA, and a narrow viewing angle of 7 degrees.

Table 1.--Technical data of LEDs

Absolute Maximum Ratings at Ta = 25 °C

DC Forward Current (mA)	Peak Forward Current (mA)	Average Forward Current (I_P = 200mA, f >= 1kHz)	Transient Forward Current (10 μs Pulse)	Reverse Voltage (I_R = 100A)
50	200	45	500	5

Electrical Characteristics at Ta = 25 °C

Fordward Voltage V_F (Volts) @ I_F =20mA		Reverse Breakdown Voltage V_R(volts) @ I_R = 100 μA		Capacitance C(pF) V_F = 0 f = 1mHz	Thermal Resistance R_θ (°C/W)	Speed of Response τ (ns)
Typ.	Max.	Min.	Typ.	Typ.		Typ.
1.9	2.4	5	25	60	220	13

Optical Characteristic at T_A = 25 °C

Luminous Intensity I_v (mcd) @ I_F = 20 mA		Peak Wavelength λ_p (nm)	Dominant Wavelength λ_d (nm)	Viewing Angle 2θ (Degrees)	Luminous Efficacy η_v (lm/w)
Min.	Typ.	Typ.	Typ.	Typ.	Typ.
1000	3000	621	615	7	263

The LEDs are driven by a special pulse power generator. The specifications of power generator (Model AV-106C-PS-P-UTA2, Avtech Electrosystems, Ottawa, Canada) is shown as Table 2.

Table 2.--Specifications of power generator

Model Destination:	AV-107C-PS-P-UTA2
Number of Channels:	4
Output Amplitude:	0 to +10 Amperes.
	One single turn amplitude control per channel.
Load Voltage Range:	0 to +100 Volts
Pulse Width:	0.5 to 20 μs.
	One ten turn locking dial control per channel
Rise, Fall Time	<= 50 ns
Channel Delay:	3 ten turn locking dial controls provided to vary delays of one with respect to next one 0 to 20 μs.
Input Trigger:	TTL, PW >= 100 ns
PRF:	<= 1Hz. Push button provided for single pulse operation
DC Mode:	Two positions switch disables pulse output and provides a 50 mA constant current to each output.

As shown in table 2, the pulse power generator has four output channels with a maximum 10 A current to drive the LEDs. Pulse width is variable from 0.5 to 20 μs. The pulse could be delayed from 1 to 20 μs between channels. A DC mode is used to adjust the optical setup. Using this power generator, we get good exposure on high-speed instant film (Polaroid type 57, ISO 3000) under 1 A current and 1 μs pulse width. Under different current and pulse width, the LED output is shown in figure 2.2. LED outputs are detected using United Detector Technology ultrafast photodetector (HS040) with a typical response

time of 0.8 ns. The photodetector is placed on the common area of light beams from four different LEDs. Frame rate is the reciprocal of interval between channels. The width of optical pulse provides the exposure time. Figure 2.2 (a) shows that the frame rate is independent of exposure time. The time delay between different channels is set to minimum. Another pulse is initiated before the previous one ends. The maximum frame rate is achieved in situation. In figure 2.2 (b), the time delay between different channels is set to maximum. The minimum frame rate is obtained in this case. Figures 2.2 (c) to (e) show examples of frame rates between minimum and maximum.

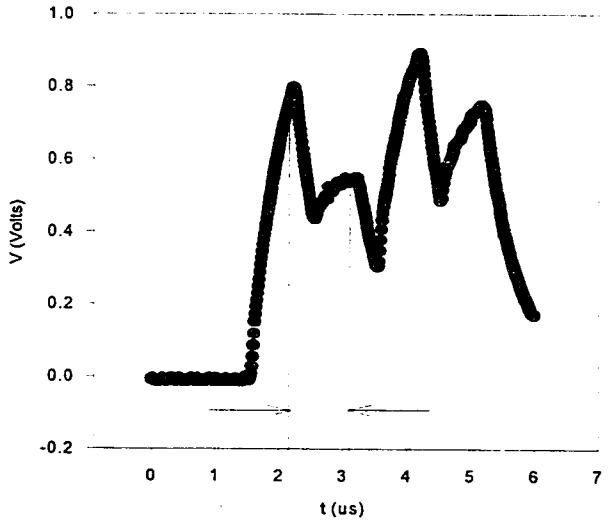

(a). Pulse current 3 A, current pulse width 1 μs, time delay between channels 0.

Corresponding frame rate 1 million frames per second, optical pulse width 1.5 μs.

Figure 2.2. LEDs outputs under different currents, pulse width and time delay

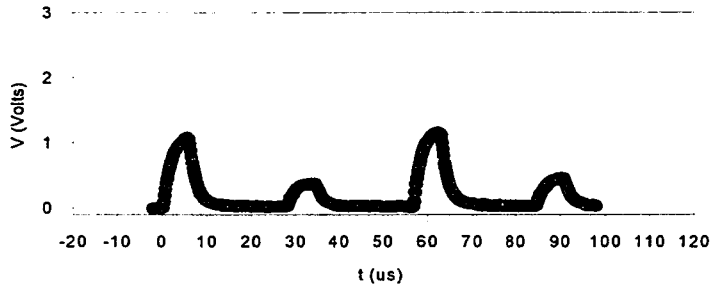

(b). Pulse current 3 A, current pulse width 8 μs, max. time delay between channel 20 μs. Corresponding min. frame rate 33000 frames per second, optical pulse width 10 μs.

Figure 2.2--continued.

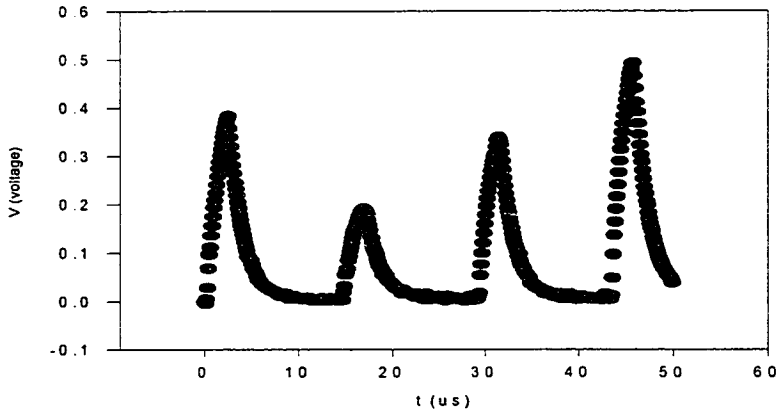

(c). Pulse current 2 A, current width 2 μs, time delay between channels 10 μs.

Corresponding frame rate 52000 frames per second, optical pulse width 4 μs

Figure 2.2--continued.

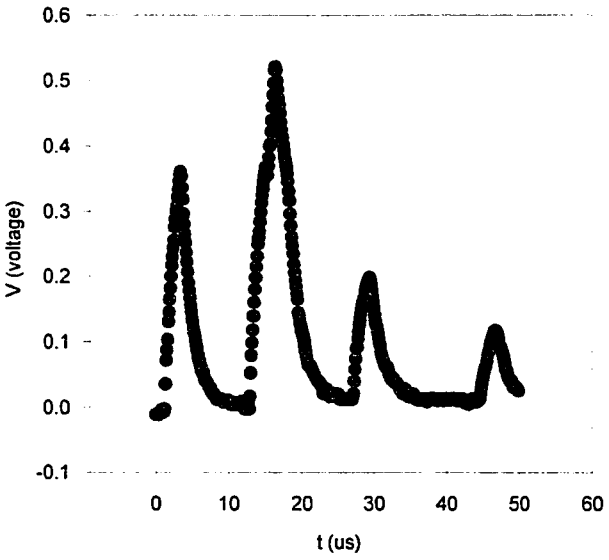

(d). Pulse current 3 A, current width 3 μs, time delay between channels 15 μs.

Corresponding frame rate 600000 frames per second, optical pulse width 5μs.

Figure 2.2--continued.

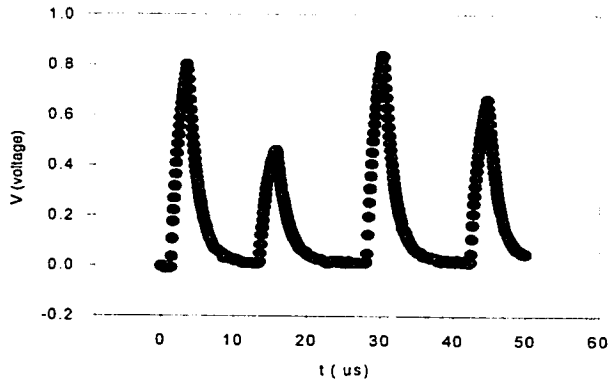

(e). Pulse current 3 A, current width 1 μs, time delay between channels 10 μs.

Corresponding frame rate 60000 frames per second, optical pulse width 2 μs.

Figure 2.2--continued.

CHAPTER THREE

OPTICAL SYSTEM ANALYSIS AND DESIGN

The Cranz-Schardin camera, introduced 60 years ago, is still a valuable tool for high-speed photography. In this camera, the light sources provide illumination and shutter functions. Image separation is accomplished with a geometric arrangement of lenses and light sources. Its intuitive principle, as illustrated in figure 1.1, is easy to understand, but its actual imaging mechanism is more complicated. There are some constraints. On the one hand, one wants to get many images on the film plane. With currently commercially available sheet film sizes, more images means smaller magnification ratio, and close arrangement and high quality of lenses. Each of the lenses will photograph the object from a different aspect. Reducing this effect requires a more compact arrangement of lenses and light sources. On the other hand, the physical dimensions of both light sources and lenses cannot be made much smaller, and in order to avoid interference of different image channels, one wants to separate the images as far as possible. LEDs as light sources make the Cranz-Schardin camera design more complicated because their weak emission requires an efficient light-gathering system. To develop a high performance camera, the designer needs to know the conjugate relationship of light sources, objective lenses, photographed object, and the film plane, and the factors that affect the magnification ratio, the size of

viewing field, and the separation of images. While much effort has been made developing light sources, the optical system itself is poorly addressed in the literature. In this chapter, we present an innovative optical system design which is efficient in light gathering and which can control the diameter of the light beam. Based on geometric optics [2], the optical system is completely analyzed. This analysis gives a design guide for optical components and their arrangements.

3.1 Conjugate Relationship

The conjugate relation of one type of Cranz-Schardin optical system using geometric optics notation is illustrated as figure 3.1. For simplicity, a two-source system is shown.

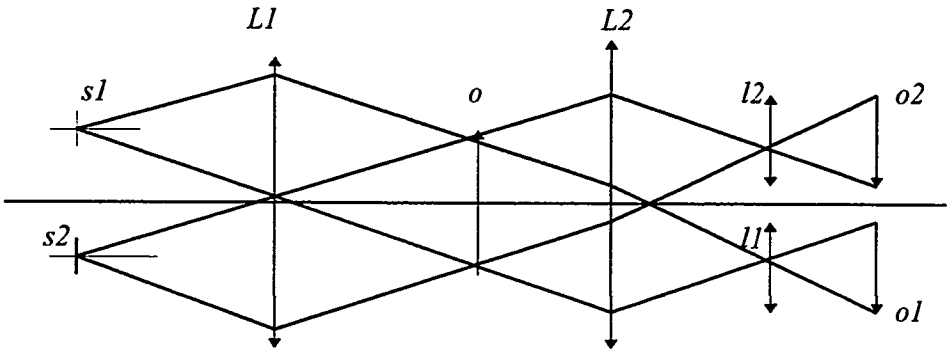

Figure 3.1. Conjugate relationship.

Light sources s1, s2 located at the focal plane of the field lens L1 are projected by lens L1 and another lens L2 onto objective l1, l2 respectively. s1 is the conjugate of

objective lens l2, that is, s1 is imaged on l2. s2 is the conjugate of objective lens l1. The object o which is to be photographed is placed between L1 and L2, and is illuminated by the projected light beam. Object o is focused onto the film by field lens L2 and objective lenses l1, l2 respectively. Without object o, the image of s1 at l2 should be a small light spot. Due to the presence of the object o, the actual image is a refraction light spot. This arrangement where the light sources are the conjugate of objective lenses makes the diameters of the objective lenses smallest. The projected light beam is a parallel light beam when the light sources are placed on the focal plane of field lens L1. Object o to be photographed is placed on the common focal plane of L1 and L2. The viewing field is decided by the common area of all light beams. With this arrangement, the largest viewing field can be achieved.

In the Cranz-Schardin system, the illumination system and imaging system are coupled closely. The basic assumption in a conventional optical system that there is a co-axis of lenses when the lenses are combined together does not exist in the Cranz-Schardin system. Thus the formation of images in a Cranz-Schardin system is hard to understand. The key to understanding the imaging mechanism is to decompose the illumination and imaging systems. Suppose that the object o does not refract light rays, then the light beams emitted from light sources s1, s2 will be transmitted through object o and form images of light sources on objective lenses l2 and l1 respectively. Suppose further that the light sources are point sources. The images of the light sources in the objective lenses are small bright spots. On the film plane, they are equally bright areas as the result of spreading of

light beams and they define the viewing field in image. The size of bright areas in the film plane determines the size of the viewing field. Actually, object o does refract light rays. Due to light scattering, the direction of light is changed by object o, and the images of light sources on objective lenses are refraction light spots whose actual shapes depend on the refraction property of object o. In order to analyze the formation of images, the scattered light is assumed to be emitted from object o. Object o is focused onto the film plane by field lens L2 and objective lenses l1, l2 respectively. Figure 3.2 illustrates the formation of the separated images. Collimated light from s1 illuminates o , and object o refracts the light beam and form image o1. Similarly collimated light from s2 also illuminates o, and the refracted light forms image o2. In figure 3.2, the dotted lines represent original light,

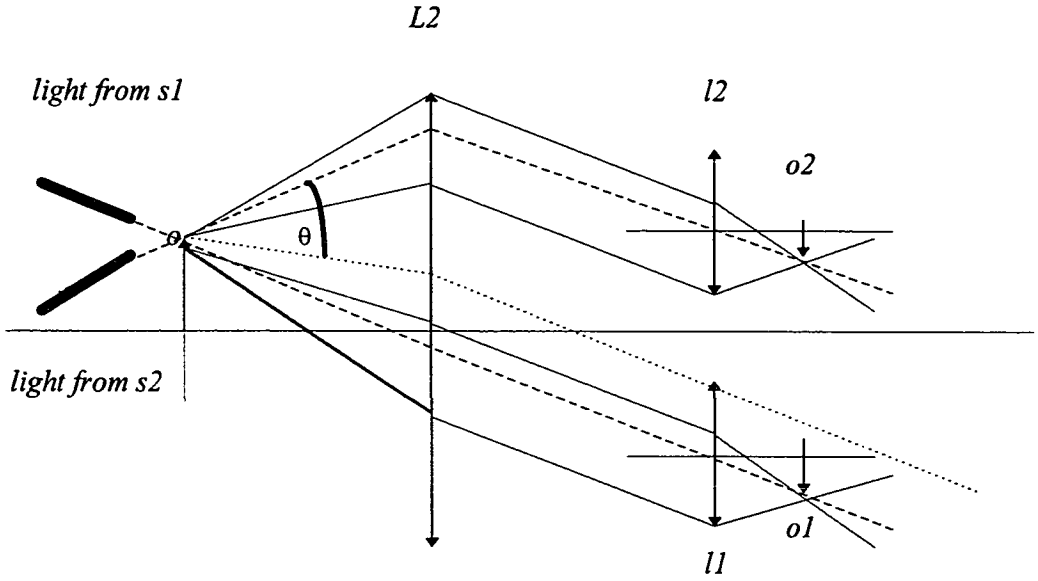

Figure 3.2. Image separation.

and the solid lines represent refracted light. Usually, refraction is not very large, and the light from s1 refracted through o will almost focus onto l1. The light from s2 refracted through o will almost focus onto l2. Large refraction will image part of light from s1 into l2, and part of light from s2 into l1, producing an overlap. As shown in figure 3.2, if the angle of refraction is larger than θ, light from light source s1 will be focused onto lens l2. This will interfere with the image from light source s2. Suppose the separation of objective lenses is 2d, and the angle from original light direction to the refracted light is θ, we have

$$\tan(\theta - \theta_0) = \frac{d - f2 * \tan\theta\, 0}{f2} \qquad (3\text{-}1)$$

where θ_0 is the angle of incidence light. So, the separation image condition is that the angle of refraction of object o is less than θ. From (3-1)

$$\theta = \theta_0 + \text{arc tan } (d/f2 - \tan\theta_0) \qquad (3\text{-}2)$$

For a given system, θ_0, d, and f2 are constant. The refraction of object to incidence light should be confined to θ to ensure a functional.

The above analysis shows why the Cranz-Schardin system is most effective in transmitted light photography, because in such applications the refraction of transmitted light is not very large. On the other hand, the refraction of reflection light is large, and the Cranz-Schardin system is not effective.

In the literature L2 is also called a field lens. This is not accurate. Field lens, by its definition, only changes the direction of light, and does not change the size of image. The

above analysis indicates that L2 definitely changes the size of the image.

3.2 Factors That Affect Magnification Ratio and the Size of Viewing Field

3.2.1 The Magnification Ratio

Suppose the object to be photographed is placed on the focal plane of L2. Under this arrangement, the conjugate relationship is shown in figure 3.3. h is the height of the object, and h′ is the height of the image. f2 is the focal length of lens L2, and f3 is the focal length of objective lens l1. From figure 3.3, we have the following relationships:

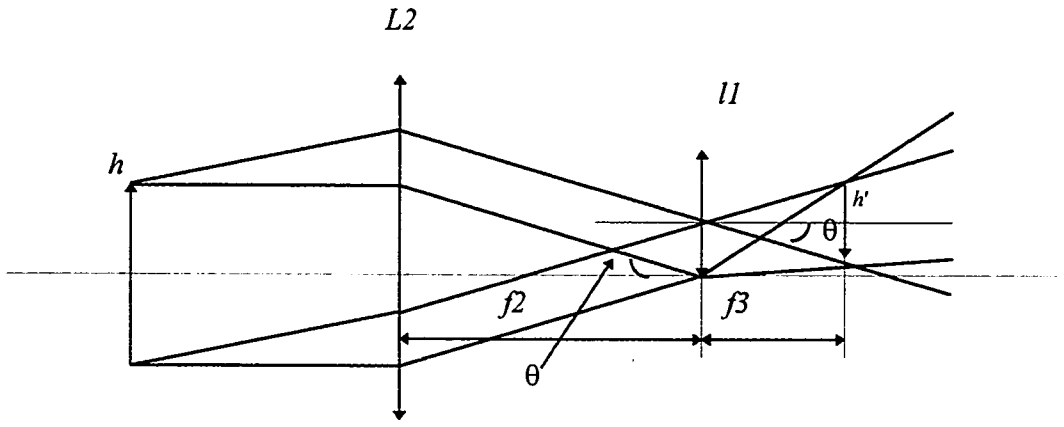

Figure 3.3. Factors that affect the magnification ratio.

$$\tan\theta = \frac{h}{2*f2} \tag{3-3}$$

$$\tan\theta = \frac{h'}{2*f3} \tag{3-4}$$

The magnification ratio is

$$\beta = \frac{h'}{h} = \frac{f3}{f2} \tag{3-5}$$

From (3-5), if we want to get a large magnification ratio, we need to increase the focal length of objective lens l1 and/or decrease the focal length of lens L2. Here are some constraints. Due to the construction of thin lenses, the longer the focal length, the larger the diameter of the lens. Thus increasing the focal length of objective lens requires increasing the diameter of the lens. If we want to get more images, we cannot increase the diameter of the lens much because it is limited by the size of available film. Decreasing the focal length of lens L2 can also increase the magnification ratio. If we want to get more images and a larger viewing field, the diameter of lens L2 should be larger. For the same reason, the focal length of L2 cannot be decreased greatly. Usually, f3 is smaller than f2, so the magnification ratio β is smaller than 1. Large magnification ratio for high-speed photography is important since high-speed films do not produce fine quality prints when enlarged. For instant film, a large magnification ratio is more important because the photographs cannot be enlarged by ordinary means.

3.2.2 Size of the Viewing Field

Suppose the size of film is W. Let the number of images in one dimension be n_r, the image size be w', the separation of objective lenses be 2d, and the size of viewing field be w. If $W \geq n_r * 2d$, to ensure that the images do not overlap,

$$w' = 2*d \tag{3-7}$$

$$w = w'/\beta \tag{3-8}$$

$$w = 2d/\beta \tag{3-9}$$

From (3-9), if we want to get a large viewing field, the image number and the magnification should be small. Thus, magnification ratio is limited by the number of images, the size of viewing field, and the structures of lenses. Under these constraints, increasing the focal length of the objective lens or decreasing the focal length of lens L2 can yield a larger magnification ratio.

3.3 Minimizing the Angle of Incidence of Light

An inherent disadvantage of the Cranz-Schardin camera is that, with each image formed by light from one and only one light source, each image will photograph the object from a different aspect. To reduce this effect, the angle of incidence of the light on both the object and the camera lenses from the optical axis of the system should be minimized. One approach to minimize the angle of incidence of light is to reduce the distance of the light sources and camera lenses. Limited by the physical dimensions of both light sources and camera lenses, the distance cannot be reduced greatly. Another approach is to increase the focal length of field lens L1.

As shown in figure 3.4, the angle of incidence of light is θ, the focal length of L1 is f1, and light source separation is 2h. Thus

$$\tan\theta = d/f1. \tag{3-10}$$

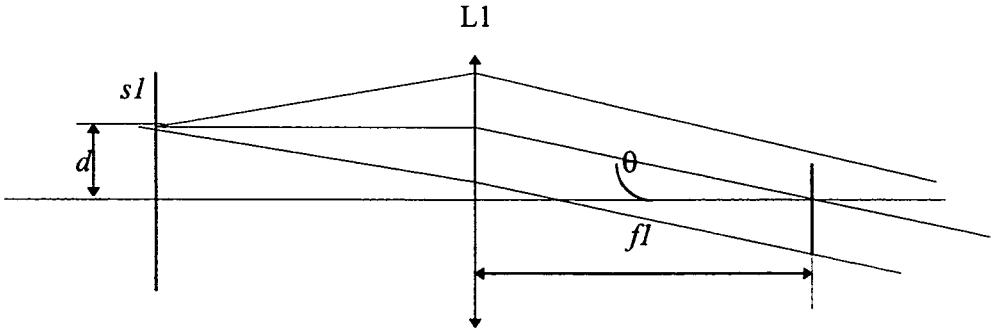

Figure 3.4. Minimizing the angle of incidence of light.

A maximum angle of incidence 4° should be acceptable. Suppose h = 76.2 mm (corresponding to a 2-in. center-to-center distance between the light sources and the camera lenses),

$$f1 = 76.2/\tan 4° = 1089.7 \text{ (mm)}$$

Some systems use a field lens with a 2000 mm focal length to reduce the angle of incidence of light. If h, the distance of sources and camera lenses can be reduced, from (3-10) the focal length of field lens L1 can be shorter. It should be noted that lenses with large focal length are expensive because they are difficult to manufacture.

Lens L2 should have the same parameters as field lens L1. At least, the diameter D of lens L2 should be the same as L1. The relative departure of a lens is defined as D/f. The manufacturing of lenses with large D/f is difficult. For a given D/f, the focal length f2 of L2 should be smaller to increase the magnification ratio. This could be formalized as:

$$D1 = D2 \qquad (3\text{-}11)$$

$$\frac{D1}{f1} \leq \frac{D2}{f2} \tag{3-12}$$

In summary, the following formulas will dominate the nature of a Cranz-Schardin camera:

$$\beta = \frac{f3}{f2} \tag{3-13}$$

$$\tan\theta = \frac{d}{f1} \tag{3-14}$$

$$D1 = D2 \tag{3-15}$$

$$\frac{D1}{f1} \leq \frac{D2}{f2} \tag{3-16}$$

$$w = 2d/\beta \tag{3-17}$$

$$n_r \leq W/2d \tag{3-18}$$

When the size of the viewing field is decided, the structures of lenses and arrangement of light sources and camera lenses are allowed, the focal length f1 of field lens L1 and the focal length f3 of objective lenses should be as large as possible, the focal length f2 of lens L2 should be as small as possible. The distances d between light sources should be as small as possible. Following these guides, one can get more images, large magnification ratio, and small angle of incidence of light for the Cranz-Schardin system.

3.4 A Light-Gathering Power System

While more efforts have been made to improve the performance of light sources, here is an approach to increase the efficiency of the light transmitted through the optical system. As shown in figure 3.5, due to the limited size of the diameters of lenses, not all

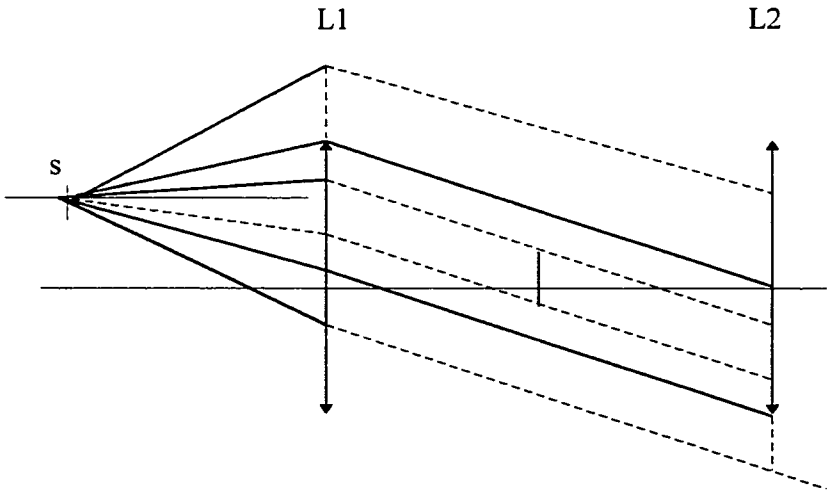

Figure 3.5. The loss of light.

light from a source is collected. Further if we just want to use a small size of the viewing field, the collected light is much less. In figure 3.5, the light between the outside dotted line and the solid line is lost due to the limitation of the size of lenses, while the light between the inside dotted line and the solid line is lost due to the fact that a small viewing field is used. Thus, on the one hand, it is important to develop intensive light sources. On the other hand, the optical system should be designed carefully to collect as much light as possible. To improve the collection of useful light, a collection lens with short focal

length is inserted between each light source and field lens L1. After the insertion of collection lenses, the light transmitted through the optical system is shown in figure 3.6. s', which is on the focal plane of field lens L1, is the virtual image of light source s formed by collect lens l. From the object, light rays emerge as if they still came from a point source placed on the focal plane of field lens L1, but the structure of light rays is changed, and the cone of light rays is greatly compacted. If the apertures of collection lenses are big enough, light from light sources can be collected completely by the collection lenses and transmitted through the optical system. This system greatly improves the efficiency of the light transmitted through the optical system. By adjusting the distances between the collection lenses and the field lens, the diameter of the light beam can be controlled, and therefore the viewing field can be controlled without changing the optical system.

The aperture of a collection lens characterizes the ability to collect light. A collection lens with a big aperture should be used to collect more light. The aperture is defined as D/f. For a practical arrangement, D cannot be large. Thus the only way to increase the aperture is to make the focal length of the collect lens shorter. And the focal length of collect lenses should be reasonably short to leave enough space to put light sources before them. If a small viewing field is required, the diameter of collection lenses should be small, and the distance between collect lenses l and field lens L1 should be short. If a large viewing field is required, the diameter of collection lenses and the distance between collection lenses l and the field lens L1 should be large.

If the diameter of collection lens is D, the focal length of collection lens is f_c, given

the size of viewing field W, the distances d and d_0 can be decided by the following formulas:

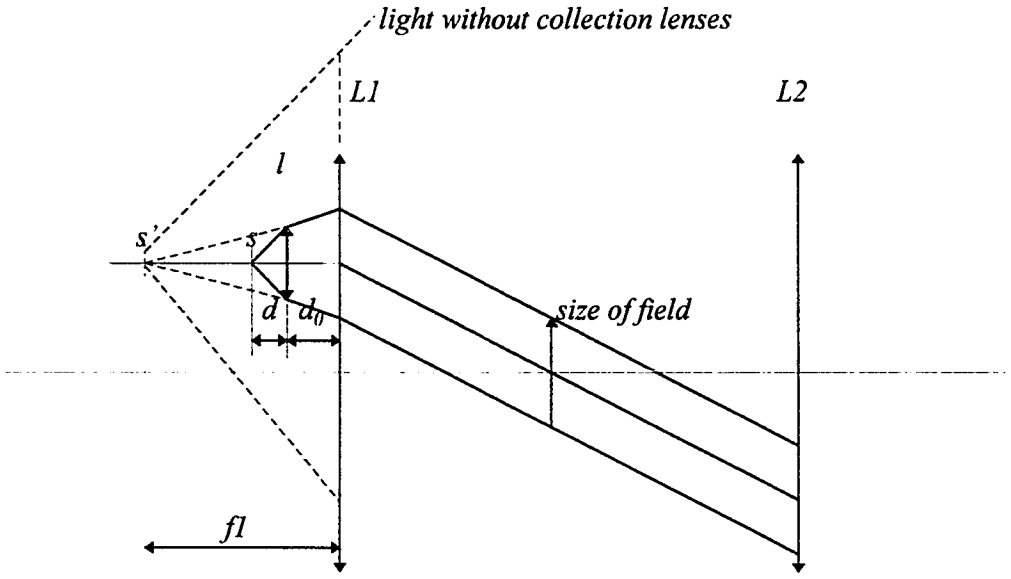

Figure 3.6 Light transmitted through optical system after insertion of collection lens.

$$\frac{1}{d} - \frac{1}{f1 - d0} = \frac{1}{fc} \tag{3-19}$$

$$\frac{W}{D} = \frac{f1}{f1 - d0} \tag{3-20}$$

From (3-19) and (3-20),

$$d0 = (1 - \frac{D}{W}) * f1 \qquad (3\text{-}21)$$

$$d = \frac{fc * f1 * D}{fc * W + f1 * D} \qquad (3\text{-}22)$$

3.5 Design Practice

With the goal to record the process of bubble collapse when a bubble interacts with a shock, based on the above analysis, we have developed a Cranz-Schardin camera using LEDs as light sources. A light-gathering power system is used. Considering the commercial availability of lenses and their cost, the parameters of lenses are chosen as follows.

Field Lens L1:

Focal length f1 = 250 mm.

Diameter D1 = 150 mm.

Plano-Convex.

Lens L2:

Focal length f2 = 250 mm.

Diameter D2 = 150 mm.

Plano-Convex.

Four Objective Lenses:

Focal length f3 = 195 mm.

Diameter D3 = 15 mm.

Plano-Convex.

Four Collect Lenses:

Focal length f0 = 15 mm.

Diameter D0 = 12 mm.

Aspheric Condenser.

Under this design, the magnification ratio

$$\beta = f3/f2 = 195/250 = 0.78$$

In the original design, the four light sources and objective lenses are arranged in a square as shown in figure 9. The angel of incidence of light

$$\text{tang } \theta = 16/250$$

$$\theta = 3^\circ .$$

The size of viewing field is 10 mm.

As discussed in 3.1, the condition that a Cranz-Schardin camera works well is that each image is formed by the light from one and only one light source. To meet this condition, the refraction of object should be small. But in our experiment, the bubble to be photographed is confined in a glass tube. Its internal diameter is 1 mm with a wall thickness of 2.5 mm. The refraction from this glass tube is so severe that it violates this condition completely as shown schematically in figure 3.7. In the revised design, the arrangement of light sources and objective lenses is staggered as shown in figure 3.9. The projection in the direction of light refraction does not cause image overlap, so even with severe refraction, the image condition is still satisfied. Under this arrangement, the size of

viewing field is increased comparing to the original arrangement.

For the revised design, the magnification rate is still 0.78. The size of viewing field is 20 mm. The angel of incidence of light is 6°.

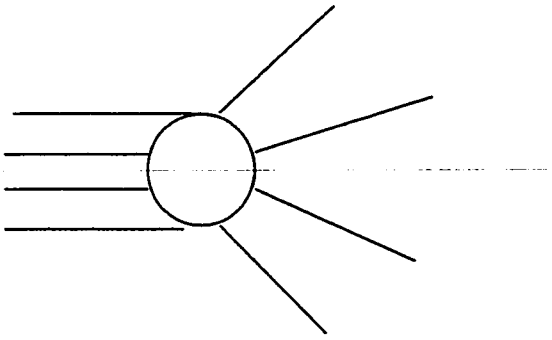

Figure 3.7. Light refraction through glass tube.

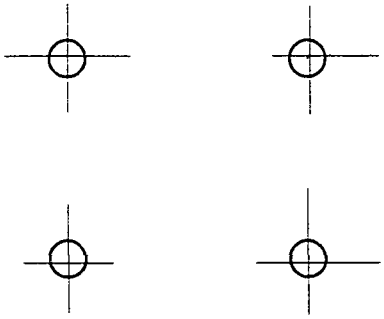

Figure 3.8. Original arrangement of LEDs and objective lenses.

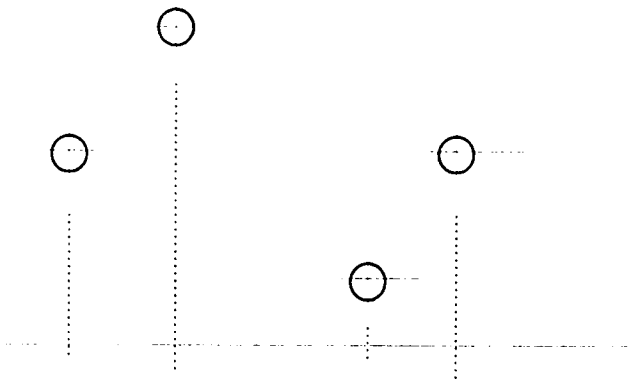

Figure 3.9. Revised arrangement of LEDs and objective lenses.

CHAPTER FOUR

MICROPROCESSOR CONTROL OF SYNCHRONIZATION

The synchronization of the Cranz-Schardin camera is a paradox. On the one hand, it is easily accomplished as the camera can be initiated with a delay of only a few micro-seconds which produced by electronic circuits rather than by mechanical components, using the same electrical signal that is used to begin the dynamic event. On the other hand, it is difficult because a Cranz-Schardin camera must capture relative few frames at extremely high framing rates. Therefore it is important to obtain an accurate synchronization signal. In this chapter, the synchronization problem is treated in more detail in the case of the high-speed interaction between a shock and a bubble.

4.1 General Description For Imaging Shock-Bubble Interaction

The timing sequence of the high-speed camera system is as follows: when a shock wave arrives and acts on the bubble, the high-speed camera is started to record the transient interaction between which lasts about 100 μs. It is extremely difficult to determine the actual moment of the arriving of shock to the bubble. A pressure transducer is mounted on the transition section between the chamber and the glass tube. The pressure transducer senses the pressure of the oncoming shock. Taking into account the distance between the

sensor and the bubble, and the speed of shock propagation in water, the microprocessor accepts the sensed analog signal of pressure as input and at a proper signal level issues a time delay in real time. After the time delay, the microprocessor outputs a pulse to trigger the high-speed camera. A block diagram illustrating the system is shown in figure 4.1. The sequence of signals is illustrated in figure 4.2. The proper trigger signal level and time delay value may be decided by referring to a theoretical fluid dynamic model and through experiments.

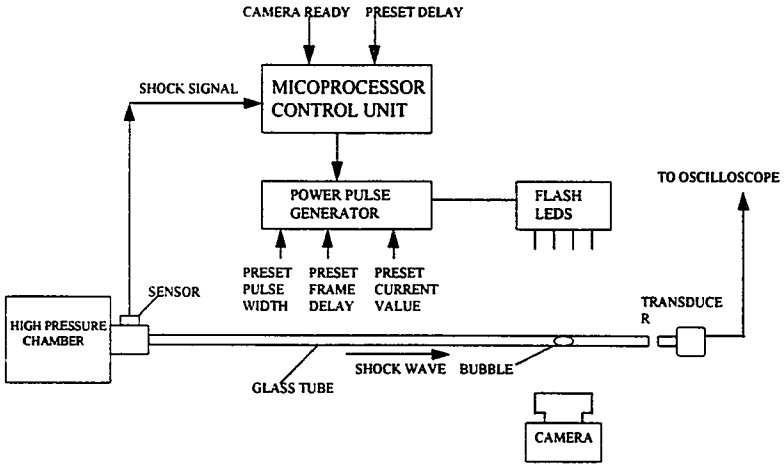

Figure 4.1. The block diagram of system components.

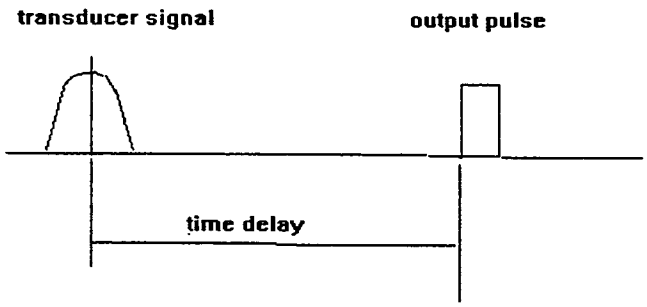

Figure 4.2. The sequence of signals.

4.2 Specific Requirements

A quartz low impedance, voltage mode subminiature pressure transducer with built-in amplifier is used for the triggering sensor. Its specifications are:

Model	PCB 105A
Pressure Range	1000 psi
Output Range	0 - 5 volts
Resolution	0.02 psi
Sensitivity	1 mV/psi
Rise Time	2 μs
Output Impedance	< 100 ohm

The signal from the transducer is shown in figure 4.3. In the experiment, the maximum output signal is about 0.8 volts. In order to increase the sensitivity and accuracy of the A/D converter, especially for the initial stage, an external amplifier is used to amplify the signal to match the A/D converter input range of 0 - 5 volts. Because of the 10 times external amplification, a limiter is used to limit the input signal under the range of the A/D converter. The original signal and the amplified signal are shown in figure 4.3.

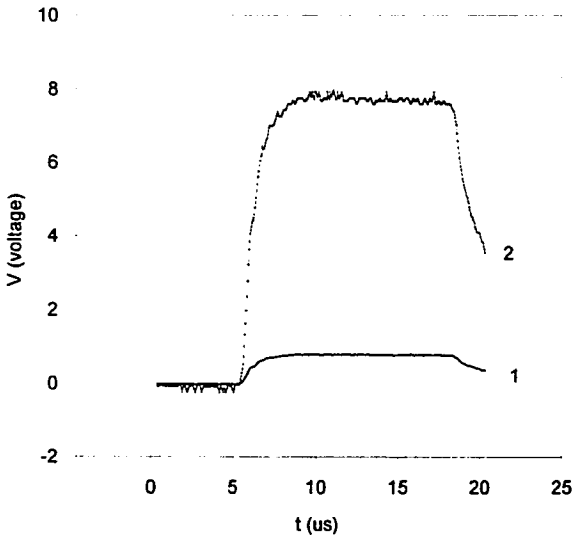

Figure 4.3. Output signal of transducer.

1: original signal; 2: Amplified signal.

The requirements of the microprocessor control synchronization system are specified below [14].

4.2.1 Input and A/D Converter Requirements

Input Range	0 - 5 V	corresponding to 0 - 1000 psi
Resolution	2.5 mV	corresponding to a pressure 2.5 psi
		corresponding to 8 bits
Conversion Time	2 μs	

The preset trigger signal level and time delay value are input through a keyboard.

4.2.2 Time Delay Requirements

The trigger signal level and time delay value are estimated from a theoretical model and modified through experiments. When the input signal reaches the trigger level, the time delay is initiated. The resolution of the time delay value is one micro-second.

4.2.3 Output Requirements

After the time delay, microprocessor control system outputs a pulse which is a TTL voltage to trigger high-speed camera. The pulse width PW >= 100 ns. The system then resets to the beginning status for the next experiment. A top level data flow diagram (DFD) is shown in figure 4.4.

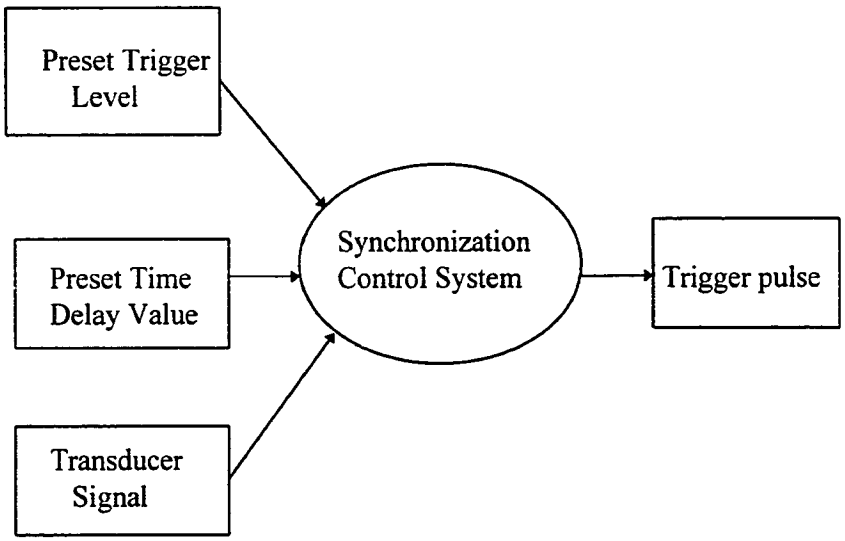

Fig. 4.4. Top level DFD

4.3 System Design

4.3.1 High Speed A/D Converter

National Semiconductor ADC0820 8-bit high speed A/D converter is used to transfer the analog signal from the pressure transducer into digital signal and couple the digital signal into MC68000 microprocessor. Key specifications of the ADC0820 are as follows:

Resolution	8 bits
Conversion Time	2.5 μs Max. (RD Mode)
	1.5 μs Max. (WR-RD Mode)

Input signals with slew rate of 100 mV/μs converted without external sample-and- hold to 8 bits

Total Unadjusted Error 1/2 LSB and 1 LSB

The ADC0820 has two basic interface modes which are selected by strapping the Mode pin high or low [15].

RD Mode

With the Mode pin grounded, the converter is set to Read mode. In this configuration, a complete conversion is done by pulling $\overline{RD}$ low until output data appears. An $\overline{INT}$ line is provided which goes low at the end of the conversion as well as a RDY output which can be used to signal a processor that the converter is busy or can serve as a system Transfer Acknowledge signal.

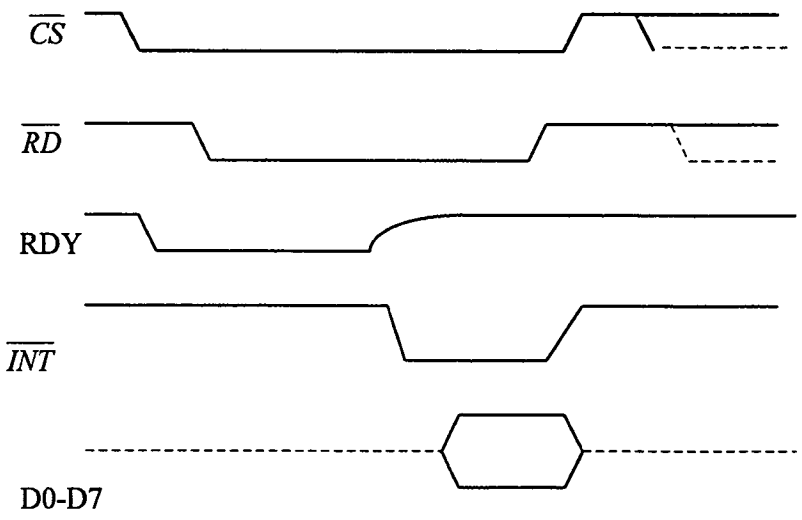

RD Mode

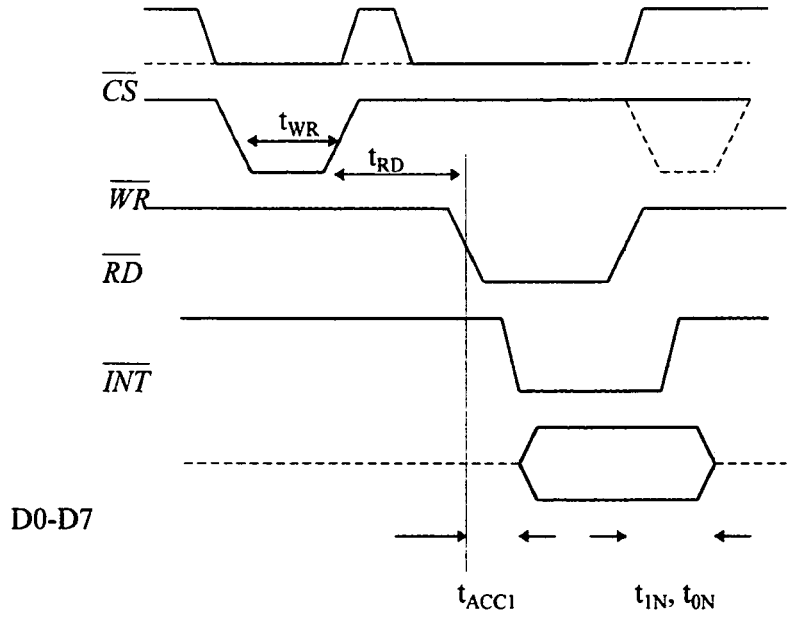

WR-RD Mode

Figure 4.5. Timing diagram for RD and WR mode.

WR then RD Mode

With the Mode pin tied high, the A/D converter will be set up for the WR-RD mode. Here a conversion is started with the $\overline{WR}$ input; however, there are two options for reading the output data which related to interface timing. If an interrupt driven scheme is desired, the user can wait for $\overline{INT}$ to go low before reading the conversion result. $\overline{INT}$ will typically go low 800 ns after $\overline{WR}$'s rising edge. However, if a shorter conversion time desired, the processor need not wait for $\overline{INT}$ and can exercise a read after only 600 ns. If this is done,

$\overline{INT}$ will immediately go low and data will appear at the output. The two modes are shown in figure 4.5.

To increase the conversion speed, the WR-RD Mode is used, that is, $\overline{WR}$ initiates a conversion, after 600 ns, $\overline{RD}$ goes low 60 ns, and then data is read from output of A/D converter. Under this configuration, the maximum conversion time is 1.5 μs. The ADC0820 is connected to MC68000 through PIT 68230. The system configuration is shown in figure 4.6.

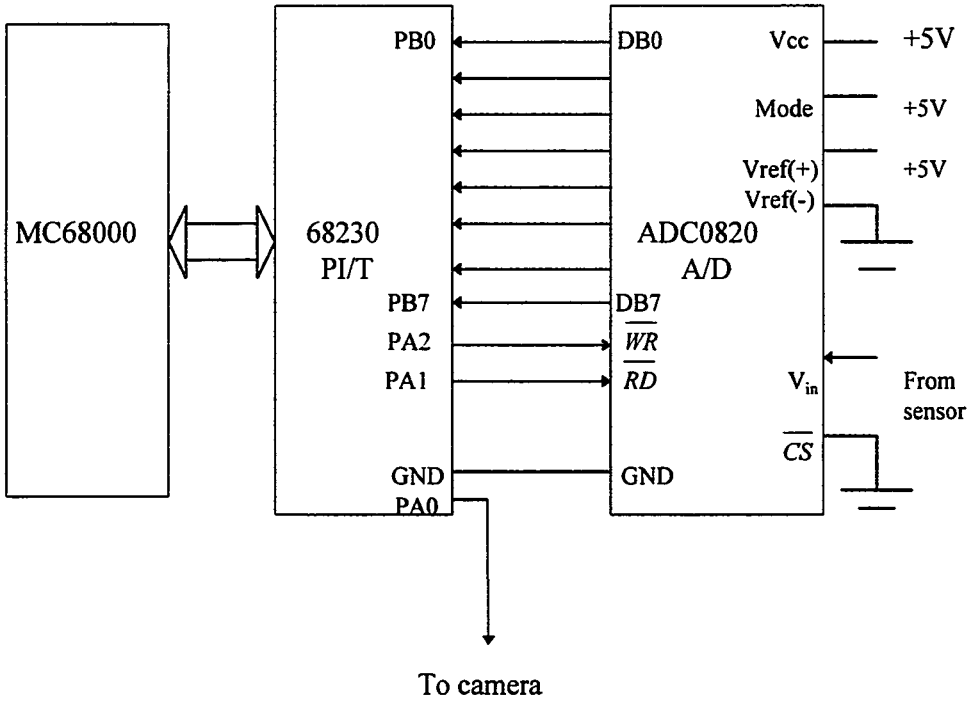

Fig. 4.6. System configuration

4.3.2 Programming the MC68000 Microprocessor

4.3.2. 1 General System Configuration

A Pentium 60 MHz PC computer as a terminal is connected to an SBC68k board through an RS232 terminal. A terminal emulation software PROCOMM supports the communication between the SBC68k and the PC. The communication parameters are set as follows:

Baud Rate 19200

8 Bits Data

No Parity

Two Stop Bits

PC Serial COMM 2

Programs in S-Format is downloaded from PC to SBC68k through PROCOMM. A resident firmware package TUTOR in the SBC68k provides a self-contained programming and operating environment. Once the program is downloaded, the TUTOR utilities can be used to debug and run the program.

4.3.2.2 The 68230 Parallel Interface/Timer (PI/T)

Port A and Port B of PI/T are configured in Mode 0, submode 1X [16]. In this mode, simple bit I/O is available in both directions. Data read from a pin programmed as an input is the instantaneous (i.e. nonlatched) signal at that pin. Data written to an output is single-buffered. Mode 0 is selected by setting bits 6 and 7 of the global register PGCR (port general control register) to 0. Submode 1X is selected by setting bits 6 and 7 of

PACR (Port A Control Register) and PBCR (Port B Control Register) to 1X. Programming Port A as all output by setting all bits of PADDR (Port A Data Direction Register) to 1. programming Port B as all input by setting all bits of PBDDR (Port B Data Direction Register) to 0. In this way, Port A will output control signals while Port B will read 8-bit data from high speed A/D converter. As shown in figure 4.7, bit 0 of Port A outputs control signal to trigger high-speed camera. Bit 1 of Port A controls of A/D converter and bit 2 of Port A controls RD of A/D converter. Bit 3 of Port A becomes high when input reaches preset trigger level and low when time runs out. This is used for adjusting experiment apparatus.

The operating mode of the timer is determined by the timer control register TCR whose format is given in table 4.1. Programming TCR in Mode 3, interrupt after time-out.

Table 4.1--Format of timer control register

Bit	TCR7 TCR6 TCR5	TCR4	TCR3	TCR2 TCR1	TCR0
Function	T_{out}/TIACK* control	ZD control	X	Clock control	Timer enable
	1 0 1	1	X		

In this mode, PC3/T_{out} is a timer function and used as a timer interrupt request output. The timer interrupt is enabled and Tout is low whenever the ZDS (zero-detect status) bit is set. PC7/TIACK* is a timer function and acknowledges interrupts generated by the timer. The timer generates an interrupt after a programmed period of time has elapsed. In MC68000, Tout is connected to INT 6 and TIACK* may be used as an interrupt acknowledge input.

The source of timing is derived from the system clock. If SZD is set, when the counter reaches zero it rolls over to its maximum value (#$FFF FFF). Figure 4.7 illustrates this process. Once the interrupt has been serviced, the host processor can halt the timer and, if necessary, read the contents of the counter. At this point, the number in the counter gives an indicator of the time elapsed between the interrupt request and its servicing.

4.3.2.3. Timing

The clock rate of MC68000 is 8 MHz. MOVE.B Instruction

MOVE.B #<data>, (An)

Table 4.2--AC Electrical Characteristics of ADC0820

Parameter	Condition	Typ	Tested limit	Design limit	Units
t_I Internal Comparison Time	Pin 7 = V_{CC}	800		1300	ns
t_{WR}, Write Time Min Max	Pin 7 = V_{CC}	 50	600		ns μs
t_{RD}, Read Time Min	Pin 7 = V_{CC}		600		ns
t_{ACC2}, Access time (Delay from Falling edge of RD to Output valid)	Pin 7 = V_{CC} $t_{RD} < t_I$	210		320	ns

takes 12 clock periods equal to 12*0.125 = 1.5 μs. Referring to the timing diagram and AC characteristics of Table 4.2, we have 600 ns < t_{WR} < 50 μs. So, the following instructions can initiate a conversion cycle. Since effective address calculation takes 4*0.125 = 1μs [17], from instruction (3) finished to instruction (4) actually reading data

from A/D converter takes at least 1 μs. This time is greater than Access Time t_{acc2} which is less than 320 ns. So Instruction (4) reads a valid data from A/D converter.

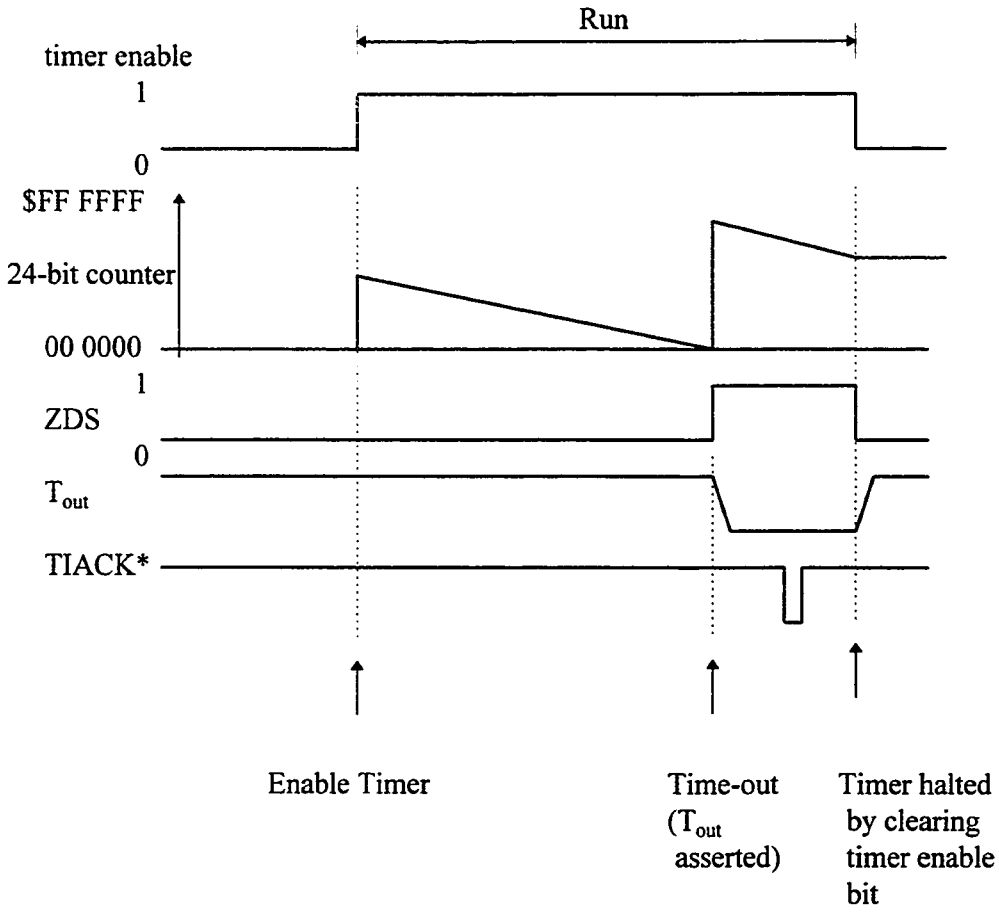

Figure 4.7. Timing diagram of PI/T as a timer-out interrupt generator.

```
MOVE.B #%XXXXX11X, PADR   ; initialize          (1)

MOVE.B #%XXXXX10X,PADR    ; WR                  (2)

MOVE.B #%XXXXX01X, PADR   ;RD                   (3)
```

```
MOVE.B Port B, D0          ; Read data from A/D converter (4)
```

4.3.3 Algorithm

The algorithm of the microprocessor control for synchronization of imaging the interaction of shock wave and bubble is given below.

Algorithm:

```
main
    begin
        input preset trigger level V0
        input preset time delay value T
        initialize I/O port
        initialize timer
        disenable timer
        repeat
            read A/D converter to D1
        until  D1 >=  V0
        Enable timer
        repeat
            wait for timer interrupt
        until doomsday
    end


interrupt subroutine
    begin
        disenable time interrupt
        output pulse
        display time-delay done
        if continue
            input trigger level V0
            input time delay value T
            repeat
                read A/D converter to D1
            until D1 >= Vo
            enable timer interrupt
            enable timer
            return
        else return to tutor
```

```
        end



initialize I/O port
        begin
                set port A to mode 0, submode 1X
                set Port A Data Direction Register to all output
                set port B to mode 0, submode 1X
                set Port B Data Direction Register to all input
                return
        end

initialize timer
        begin
                clear interrupt
                store interrupt subroutine address
                set timer control register to mode 3 (interrupt after time-out)
                disenable timer
                set low 8-bit of time delay value to low 8-bit of
                        counter preload register (CPRL)
                set middle 8-bit of time delay value to middle 8-bit of
                        counter preload register (CPRM)
                set high 8-bit of time delay value to high 8-bit of
                        counter preload register (CPRH)
                return
        end

input trigger level
        begin
                accept input in decal point form X.XXX
                remove decal point
                convert input from ASCII to hex
                trigger level in binary form = ((V0/Vref)*256)/1000
                retrun
        end

input time delay value
        begin
                accept input from key board
                convert input from ASCII into hex
                store time delay value
```

```
        return
end
```

The source code which is coded in MC68000 assembly language is given in appendix 1.

4.4 Uncertainty of Time Delay Analysis

For the system, the sources of errors come from (1) transducer measuring error, (2) A/D converter error, (3) time delay error, and (4) trigger delay erroror. Trigger delay error, which is propagation delay during signal propagates through control circuits, is a system error, can be removed. Transduer measuring error and A/D converter error are dependent on pressure and can be ignored compared to the error from determining trigger level. Time delay error from the limited clock rate and instruction execution time is analysis as follows.

Let us consider some code producing the error.

(1) Error from read A/D converter

```
POLLING:                                    CLOCK CYCLE
        MOVE.B    #%11111100, PADR          12
        MOVE.B    #%11111110, PADR          12
        MOVE.B    #%11111010, PADR          12
        CMP.B     PBDR, D1                  6
        BGT       POLLING                   10
```

(2) Error from waiting for timer interrupt

```
WAIT:   BRA  WAIT                           10
```

For error from reading A/D converter, total clock cycles T = 52, $\Delta t1 = 52*0.125 = 6.5\ \mu s$.

For erroe from waiting timer interrupt, clock cycles T = 10, $\Delta t2 = 10*0.125 = 1.25\mu s$.

For a time delay 100 μs, the rms error:

$\Delta t1/t = 6.5/100 = 0.065$

$\Delta t2/t = 1.25/100 = 0.0125$

$$\Delta t / t = \sqrt{\left(\Delta t_1 / t\right)^2 + \left(\Delta t_2 / t\right)^2} = 0.066 = 6.6\%$$

$\Delta t = 0.066 * 100 = 6.6\ \mu s$

This error is smaller compared to the error from determining trigger level. Therefore, the accuracy of time delay is consider satisfied.

CHAPTER FIVE

EXPERIMENT PROCEDURE

The experimental procedure is to capture and image the high speed process of the interaction of shock wave and bubble using the custom-built high-speed camera. The acceptability of this camera is examined through this application.

5.1 Test Equipment and Instrumentation

The schematic of the experiment arrangement is shown as figure 4.1. In addition to the pressure transducer at the exit of the high-pressure chamber, another transducer is installed at the other end of the glass tube to measure the time for shock to propagate along the glass tube. A bubble is implanted in the water-filled tube by using a syringe.

5.1.1 The Micro Shock Tube And Behavior Of The Valve

In the experiment, the micro shock tube is not built like a gun which uses explosives to generate shock waves because the spark produced will expose the film. The micro shock tube illustrated in figure 4.1 consists of an aluminum chamber and a driven tube (Pyrex capillary tube), and a transition section to install a pressure transducer. The shock wave is produced by opening a solenoid valve electrically. When the solenoid valve opens, high pressure air in the chamber is expelled and produces a shock wave.

The compressed air is regulated in the chamber from a high pressure bottle. The chamber has a hollow cylindrical interior with an inner diameter of 100.8 mm and a width of 50 mm. The driven section is made up of a transparent Pyrex capillary tube with an outer diameter of 6 mm, and an inner diameter of 1.01 mm.

When the valve is switched on, it opens in a finite time until the maximum opening is achieved. The maximum opening will last for some time and then the valve closes. Corresponding to the transition process of the valve opening, the pressure of shock wave measured by pressure transducer is shown in figure 5.1. When the opening is small, the shock strength is too weak to cause severe interaction on the bubble. A threshold value must be determined. Above this value, the shock wave will act on and damage the bubble.

5.1.2 Trigger Pulse

The solenoid valve of shock tube and the data acquisition system are triggered simultaneously. The pulse is generated by a simple 555 timer circuit. Since the shock tube is fired by opening the valve electromagnetically, the pulse will open the valve for a duration t. Thus the pulse is able to control the volume of gas flowing into the Pyrex tube and the arming of the oscilloscope. Due to the large variability of the valve opening, the pulse signal is not suitable to be used as synchronization for high-speed camera.

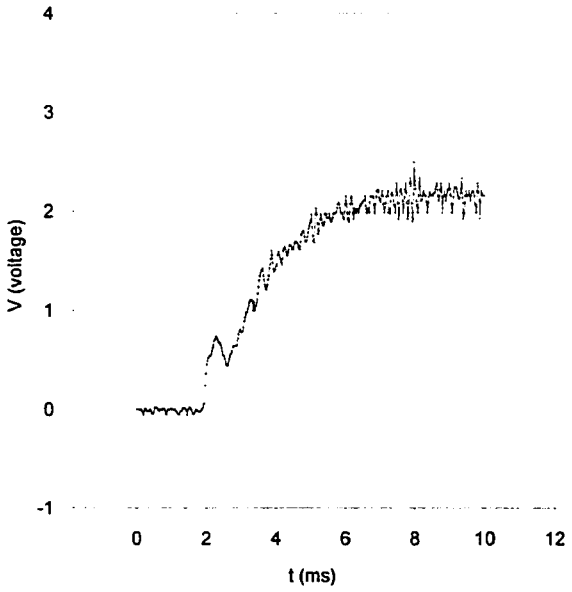

Figure 5.1. Transition process of the valve opening.

5.1.3 Data Acquisition Hardware

Since the propagation of shock wave along the Pyrex is a fast process, the speed of data acquisition hardware must be fast enough used to record this process. A high-speed digital oscilloscope (HP 5442A) is used to ensure this. The HP 5442A is a digital oscilloscope with full HP-IB programmability and it can sample at 2 Gsa/s. This sampling speed is more than sufficient for this experiment with an expected maximum signal frequency in the kHz range. The triggering and data acquisition signal flow is illustrated in

figure 5.2. A Pentium 60 MHz personal computer is connected to the HP 5442A. The PC can be used to retrieve the data stored in the digital oscilloscope through HP VEE (Hewlett Packard Visual Engineering Environment) software. With the PC, the retrieved data can be manipulated and analyzed. However, it is much faster to use disk to transfer the data stored in the oscilloscope to PC.

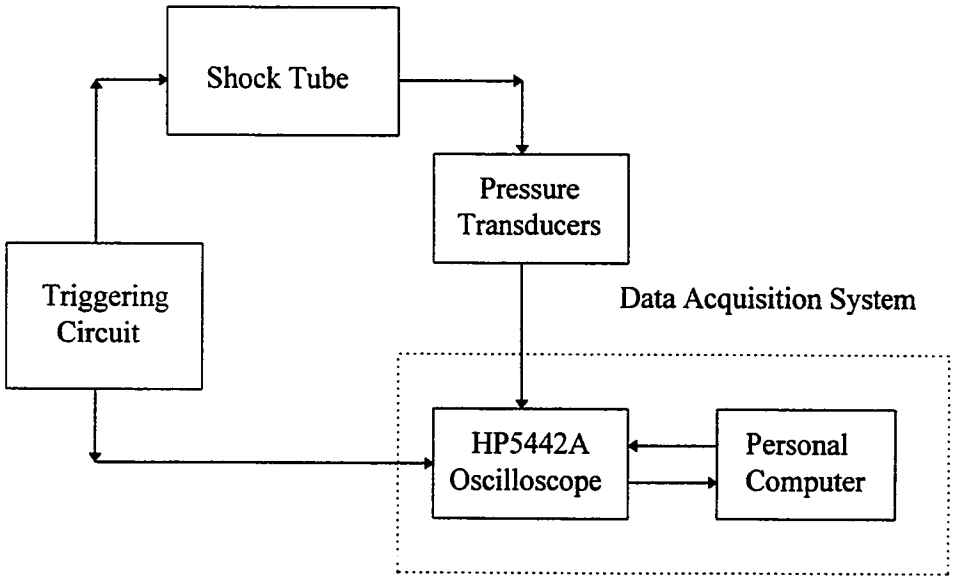

Figure 5.2. Block diagram of data acquisition signal flow.

5.1.4 High-speed Camera

The high-speed camera described in above chapters is applied in the experiment.

5.2 Experimental Procedure

5.2.1 Determine The Trigger Level And Time Delay Value

The trigger level should not be too small or large. A small trigger level will require unreasonably long time delay which results in bad synchronization. A large trigger level will result in too small a time delay to capture the bubble image.

Two transducers are used, one installed in the chamber end, the other one installed at the open end. The propagation time of shock wave along the shock tube is measured by the signals from the two transducers and observed through the HP 5442A oscilloscope. Figure 5.3 shows that the propagation time of the shock wave under the pressure of 300 psi is about 0.8 ms.

Suppose a small trigger signal level *v1* is selected, and further suppose that the pressure producing strong enough shock wave to damage the bubble is in signal level *v2*, and $v2 > v1$. The time delay consists two parts: (1) $\Delta t1$, the propagation time of the shock wave along the glass tube, and (2) $\Delta t2$, the time delay from signal *v1* rising to signal *v2*, that is, $\Delta t = \Delta t1 + \Delta t2$. In the experiments, the time delay is actually determined in this way.

5.2.2 Image Bubble

The synchronization control program is downloaded from the PC to MC68000 using PROCOMM. Entering the GO 1000 command starts the program. The computer will prompt for entering the trigger level and the time delay value in micro-seconds. When this is done, the computer will wait for a signal to trigger the camera.

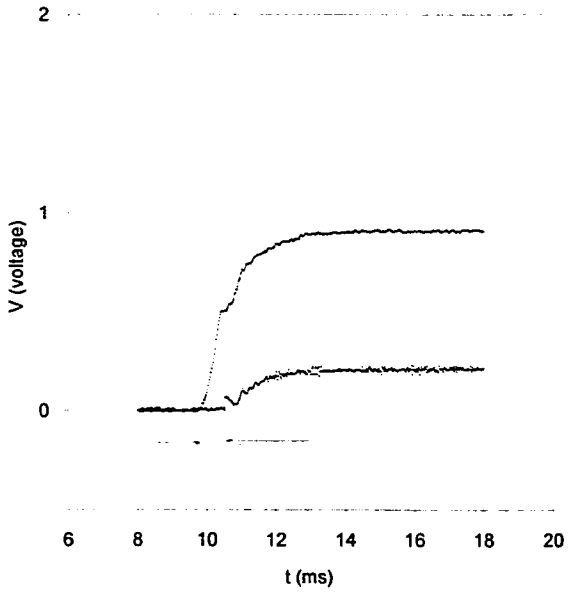

Figure 5.3. The propagation time of shock wave along the tube.

Turn mode selection button to the DC mode. Implant a bubble and place it on the center of viewing field using syringe. Adjust optical system and make the images of bubble best. Turn mode selection button to pulse mode to wait for triggering.

The experiment is initiated by pushing switch button of a 555 timer circuit. A pulse is generated to fire the shock tube by opening the valve electromagnetically. When the valve opens, the shock wave is generated. When the pressure transducer senses the

pressure signal, time delay is initiated, and then the camera is triggered. An exposure of four-bubble image is formed on the film.

The interval between different channels is set to a maximum, that is 10 μs as in the camera. The pulse current is adjusted to produce suitable exposure on the film. The measured shock wave propagation time from the transducers is input to computer as initial time delay value. A binary search is carried out to find proper time delay value.

CHAPTER SIX

RESULTS AND CONCLUSIONS

6.1 Cavitaion Experiments Results

Using the Cranz-Schardin high-speed camera and microprocessor synchronization control system, we have carried out preliminary cavitation experiments. The goals of this experiment are to capture and image bubble behavior when a shock wave acts on it, and to examine the acceptability of the high-speed camera. In a experiment, the pressure is 300 psi. For comparison, repeated exposure is used. The first exposure is the images of a bubble in the undisturbed state. The bubble is placed at the center of the viewing field. The second exposure is the dynamic images of a bubble when a shock wave acts on it. The trigger level is 2 volts, corresponding to a pressure of 200 psi measured at the transducer. The time delay is set to 1.25 ms. The time interval between different channels is 20 μs, exposure time is 6 μs. The driving currents for LEDs are 2.5 A. From the picture, the bubble is moving and becomes smaller. The moving distance is smaller in the first frame, and larger in the last frame. Under the experiment condition, the process of interaction between the shock and the bubble is not very fast compared to the speed of high-speed camera. Because of the property of the valve, a weak shock wave which is not strong enough to damage the bubble is formed. The weak shock wave pushes the bubble and

makes the bubble moving outside the viewing field. These are considered to be reasons that we did not observe bubble destruction.

6.2 Conclusions and Recommendations

A Cranz-Schardin high-speed camera with a speed of one million frames per second has been successfully developed. LEDs as light sources, innovative design of efficient light-gathering system, and microprocessor control for synchronization are among the features of this camera. Its acceptability is examined through cavitation experiments. Although the motivation to develop this camera is to provide a low cost and high-speed optical method for cavitation study, this camera is an excellent high-speed recording instrument for transmitted light photography with a wide range of applications. The analysis for the optical system of Cranz-Schardin camera is original. It provides a valuable guide for the design of this kind of camera which is not available in the literature. LEDs are chosen as light sources. Their advantages are compactness, low cost, ease of control. LED can work in continuous or pulse modes. The continuous mode is convenient for optical adjustment. Although the developed microprocessor control of synchronization is geared toward cavitation studies, this control method is flexible, and can be adapted for other applications.

Even though much effort has been made to develop the camera, many improvements may be incorporated for a future version. Only four frames are available in the current design. Up to 24 frames can be made to provide for a longer observation period

at higher framing rates. The frames can be arranged in a 4 by 6 array to take advantage of the aspect ratio of the rectangular instant film. The pulse width, currents and delay between different channels are controlled by the pulse generator in the current design. This can be done by microprocessor. Especially, in the current camera, the delay between different channels is set a maximum of 20 μs. This is not convenient for adjusting synchronization, and is too fast for the process to be studied. Using microprocessor control, a wide range can be achieved which is critical for synchronization. It is possible to obtain a repeat exposure using microprocessor control. Currently, the optical lenses are selected from commercially available products. Their cost are low, but the image qualities are poor, especially, the field curvature is very severe at large viewing angles. Special designs of the lenses for the purpose of Cranz-Schardin camera can be made to increase the quality of images. Finally, using instant film saves studio work, it also causes difficulty in enlarging pictures. A large magnification ratio system can produce larger pictures. Alternatively, a digital imaging system can be used for recording and facilitate computerized post-processing.

APPENDIX

SOURCE CODE

```
        ORG   $1000
START:
        MOVE.B      #0,D1
        BSR         PRESET_TRIGGER
        BSR         PRESET_DELAY
        BSR         INITCLK             ;INITIALIZE TIMER
        BSR         INITPORT            ;CONFIGURE PIT PORT
        MOVE.B      #%11111110,PADR     ;SET 0 TO PORT A BIT 0

POLLING:
        MOVE.B      #%11111100,PADR     ;OUT_PUT 0 TO PORT A BIT 1
        MOVE.B      #%11111110,PADR     ;OUT_PUT 1 TO PORT A BIT 1
        MOVE.B      #%11111010,PADR     ;OUT_PUT 0 TO PORT A BIT 2
        NOP
        CMP.B       PBDR,D1             ;COMPARE INPUT WITH PRESTE
                                        ;VALUE
        BGT         POLLING             ;INPUT < PRESTE VALUE, LOOP

        MOVE.B      #%10110001,TICR     ;ENABLE CLOCK TO START TIMER
        MOVE.B      #%11111110,PADR     ;OUTPUT 1 TO PORT A BIT 3
WAIT:
        BRA         WAIT                ;WAIT FOR TIMER-OUT INTERRUPT
INITCLK:
        AND.W       #$F8FF,SR           ;CLAER INTERRUPTS
        MOVE.L      #CLKINT,VECTAD      ;STORE INTERRUPT SERVICE ADDRESS
        MOVE.B      #VECTNO,TIVR        ;STORE INTERRUPT NO
        MOVE.B      #%10110000,TICR     ;SET TIMER CONTROL REGISTER TO
                                        ;MODE 3 (INTERRUPT AFTER TIMER-
                                        ;OUT). AT THIS POINT,
                                        ;TIMER DISENABLE
        RTS

INITPORT:
        MOVE.B      #$00,PGCR           ;SET PORT GENERAL CONTROL
                                        ;REGISTER TO MODE 0
        MOVE.B      #$C0,PACR           ;SET PORT A CONTROL REGISTER
                                        ;TO SUBMODE 1X
        MOVE.B      #$C0,PBCR           ;SET PORT B CONTROL REGISTER
                                        ;TO SUBMODE 1X
        MOVE.B      #$FF,PADDR          ;SET PORT A DIRECTION REGISTER
```

```
                                    ;TO ALL OUTPUT
        MOVE.B      #$00,PBDDR      ;SET PORT B DIRECTION REGISTER
                                    ;TO ALL INPUT
        RTS
CLKINT:
        OR.W        #$0700,SR
        MOVE.B      #$FF,PADR       ;OUTPUT 1 TO PORTA DATA REGIST
                                    ;BIT 0
        MOVE.L      #$7FFF,D0       ;LOOP FOR PULSE WIDTH
LOOP:
        SUB         #1,D0
        BNE         LOOP
        MOVE.B      #$0,PADR    ;TERMINATE PULSE OUTPUT
        LEA         DBUFFER,A5
        LEA         PASSONE,A6
        MOVE.B      #243,D7
        TRAP        #14

        MOVE.B      #228,D7
        TRAP        #14
        RTE

PRESET_DELAY:
        LEA         M01,A5
        LEA         M11,A6
        MOVE.B      #243,D7
        TRAP        #14
        LEA         INBUFFER,A5
        LEA         INBUFFER,A6
        MOVE.B      #241,D7
        TRAP        #14

        MOVE.B      #225,D7
        TRAP        #14

        LSR.L       #2,D0
        MOVE.B      D0,CPRL
        LSR         #8,D0
        MOVE.B      D0,CPRM
        SWAP        D0
        MOVE.B      D0,CPRH
        RTS
```

```
PRESET_TRIGGER:
        LEA         PROMPT,A5
        LEA         PROMPT1,A6
        MOVE.B      #243,D7
        TRAP  #14

        LEA         IN_DATA,A5
        LEA         IN_DATA,A6
        MOVE.B      #241,D7
        TRAP        #14

        MOVE.B      #225,D7
        TRAP        #14

        MOVE.B      D0,D1
        ANDI        #$00FF,D1
        RTS

M01:        BYTE   'PLEASE ENTER TIME DELAY VALUE IN MICRO-
                   SECOND: ',$0D,$0A
M11:        BYTE   1
PROMPT:     BYTE   'PLEASE ENTER TRIGGER VALUE BETWEEN 1-255:
                   ',$0D,$0A
PROMPT1:    BYTE   1
INBUFFER:   BLKB   40
IN_DATA:    BLKB   40

            ORG    $3000
DBUFFER:    BYTE   'TIME DELAY DONE',$0D,$0A
PASSONE:    BYTE   1

VECTNO:     EQU    $40          ;DEFINE TIME-OUT INTERRUPT NO
VECTAD:     EQU    VECTNO*4     ;INTERRUPT SERVICE ADDRESS

PADDR:      EQU    $FE8005      ;PORT A DATA DIRECTION REGISTER
PBDDR:      EQU    $FE8007      ;PORT B DATA DIRECTION REGISTER
PGCR:       EQU    $FE8001      ;PORT GENERAL CONTROL REGISTER
PACR:       EQU    $FE800D      ;PORT A CONTROL REGISTER
PBCR:       EQU    $FE800F      ;PORT B CONTROL REGISTER
PADR:       EQU    $FE8011      ;PORT A DATA REGISTER
PBDR:       EQU    $FE8013      ;PORT B DATA REGISTER
```

```
TICR:     EQU   $FE8021     ;TIMER CONTROL REGISTER
TIVR:     EQU   $FE8023     ;TIMER INTERRUPT VECTOR REGISTER
CPRH:     EQU   $FE8027     ;COUNTER PRELOAD REGISTER HIGH
CPRM:     EQU   $FE8029     ;COUNTER PRELOAD REGISTER MIDDLE
CPRL:     EQU   $FE802B     ;COUNTER PRELOAD REGISTER LOW
          END   START
```

REFERENCES

1. Dubovik, A. S., Photographic Recording of High-speed Processes, Pergamon Press, 1968.
2. Hyzer, W. G., Engineering and Scientific High-speed Photography, The Macmilan Company, 1962.
3. Cranz, C. and Schardin, H., "Kinematographie auf ruhendem Film und mit extrem hoher Bildfrequenz," Zs. Physik, Vol. 56, 1929, pp. 147-183.
4. Dally, J. W. and Sanford, R. J., "Multiple Ruby Laser System for High Speed Photography," Optical Engineering, Vol. 21, No. 4, 1982, pp. 704-708.
5. Courtney-Partt, J. S. and Thackeray, D. P. C., "High-speed Silhouette Micrography Using Image-splitting Techniques," Proceedings of the Third International Congress on High-speed Photography.
6. Dally, J. W. and Brillhart, L. V., "Application of the Multiple-Spark-Gap Camera to Dynamic Photoelasticity," Journal of the SMPTE, Vol. 77, 1968, pp. 116-120.
7. Dally, J. W. and Sanford, R. J., "A New High Speed Photographic System For Experimental Mechanics," Mechanics Research Communications, Vol. 9, No. 5, 1982, pp. 337-341.

8. Stasicki, B., Hiller, W. J. and Meier, G. E. A., "Light Pulse Generator for High Speed Photography Using Semiconductor Devices as a Light Source," Optical Engineering, Vol. 29, No. 7, 1990, pp. 821-827.

9. Stasicki, B. and Meier, G. E. A., "Miniaturized Semiconductor Light Source System for Cranz-Schardin Applications," 19th International Congress on High-Speed Photography and Photonics, SPIE Vol. 1358, 1990, pp. 1222-1227.

10. Bretthauer, B. Meier, G. E. A. and Stasicki, B., "An Electronic Cranz-Schardin Camera," Review of Scientific Instruments, Vol. 62, No. 2, 1991, pp. 364-368.

11. Hiller, W. Lent, H. M., Meier, G. E. A. and Stasicki, B., "A Pulsed Light Generator for High Speed Photography," Experiments in Fluids, No. 5, 1987, pp. 141-144.

12. Sanford, R. J. and Dally, J. W., "Applications of a Reflective Mode Cranz-Schardin Optical System to Dynamic Fracture and Stress Analysis," Proceedings of the 37th International Instrumentation Synsposium, San Diego, CALF., May, 5-9, 1991, pp. 63-73.

13. Fujikawa, S. and Akamatsu, T., "Experimental Investigations of Cavitation Bubble Collapse by a Water Shock Tube," Bulletin of the JSME, Vol. 21, No. 152, 1987, pp. 223-230.

14. National Semiconductor, National Data Acquisition Databook, 1995 Edition.

15. Fairley, R. E., Software Engineering: A Practitioner's Approach, 3rd Edition, McGraw-Hill, Inc., 1992.

16. Alan Clements, Microprocessor System Design, PWS-Kent Publishing Co., 2nd Edition, 1992.

17. Motorola, M68000 8-/16-/32-bit Microprocessors User's Manual, Prentice Hall, Eight Edition, 1991.